Article

Molecular Modeling of Exquisitely Selective c-Met Inhibitors through 3D-QSAR and Molecular Dynamics Simulations

Haoliang Yuan,[†,‡] Jin Zhuang,[‡] Shihe Hu,[‡] Huifang Li,[§] Jinxing Xu,[‡] Yaning Hu,[‡] Xiao Xiong,[‡] Yadong Chen,*[,‡] and Tao Lu*[,‡,ξ]

[†]Key Laboratory of Nuclear Medicine, Ministry of Health, Jiangsu Key Laboratory of Molecular Nuclear Medicine, Jiangsu Institute of Nuclear Medicine, Wuxi, 214063 Jiangsu, P. R. China

[‡]Laboratory of Molecular Design and Drug Discovery, School of Basic Science, China Pharmaceutical University, 24 Tongjiaxiang, Nanjing, 210009 Jiangsu, P. R. China

[ξ]State Key Laboratory of Natural Medicines, China Pharmaceutical University, 24 Tongjiaxiang, Nanjing, 210009 Jiangsu, P. R. China

[§]Vancouver Prostate Centre, University of British Columbia, 2660 Oak Street, Vancouver, British Columbia V6H 3Z6, Canada

S *Supporting Information*

ABSTRACT: c-Met has been considered as an attractive target for developing antitumor agents. The highly selective c-Met inhibitors provide invaluable opportunities for the combination with other therapies safely to achieve the optimal efficacy. In this work, a series of triazolopyrazine c-Met inhibitors with exquisitely selectivity were investigated using a combination of molecular docking, three-dimensional quantitative structure–activity relationship (3D-QSAR), and molecular dynamics simulation. Comparative molecular field analysis

(CoMFA) and comparative molecular similarity index analysis (CoMSIA) models were developed to reveal the structural determinants for c-Met inhibition. Both models were validated to have high reliability and predictability, and contour map analysis suggested feature requirements for different substituents on the scaffold. It is worth noting that an important hydrogen bond rich region was identified in the unique narrow channel, which is distinct from other kinases. Molecular dynamics simulations and binding free energy calculations provided further support that suitable groups in this hydrogen bond rich region made great contributions to the binding of ligands. Moreover, hydrogen bonds with residues of the narrow channel were also indicated to be essential to improve the activity and selectivity. This study will facilitate the discovery and optimization of novel c-Met inhibitors with higher activity and selectivity.
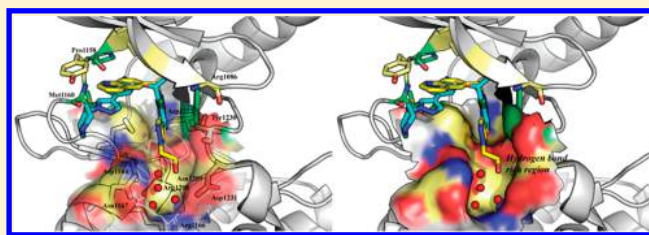
1. INTRODUCTION

Mesenchymal-epithelial transition factor (c-Met), a member of receptor tyrosine kinase (RTKs), together with its natural ligand, hepatocyte growth factor (HGF), play a critical role in cell proliferation, migration, and invasion, which are essential for normal embryonic development, wound healing, and tissue regeneration.[1,2] Aberrant HGF/MET signaling pathway occurs in virtually a number of human cancers, such as liver, breast, pancreas, lung, kidney, bladder, ovary, brain, prostate, and other cancers,[3] and overexpression of MET and/or HGF is associated with high tumor grade and poor prognosis.[4−6] Several mechanisms lead to the dysregulation, including the overexpression of c-Met and/or HGF, amplification of the *Met* gene, and activating mutations of c-Met. The up-regulation of HGF and/or MET in tumor microenvironment may cause resistance to the effects of anticancer kinase inhibitors, highlighting the important role for HGF/MET inhibitors in cancer therapy.[7] Furthermore, it was reported that the aberrant activation of HGF/MET signaling confers resistance of EGFR[8] and BRAF[9] kinase inhibitors.[10] Due to the important role of aberrant HGF/MET signaling in human cancer oncogenesis,

invasion/metastasis, and resistance to cancer therapies, the inhibition of HGF/MET signaling represents great potential in cancer treatment.[11] Intensive interests in inhibiting the HGF/MET pathway have been fueled by continually emerging evidence of clinical benefits in a variety of cancers.[12−15] Developing small-molecule c-Met kinase inhibitors is a viable approach toward modulating HGF/MET signaling in human clinical study of cancers.

There have been a number of studies on developing small molecule c-Met inhibitors, and various c-Met inhibitors have been reported.[14−23] A series of c-Met inhibitors based on the structural scaffold of triazolopyrazine, represented by PF-04217903, demonstrated exquisite c-Met kinase selectivity. PF-04217903 has advanced into human clinical studies on oncology.[22] The highly selective c-Met inhibitors provide invaluable opportunities for the combination with other therapies safely to achieve the optimal efficacy. Another inhibitor, Crizotinib (PF-02341066), which is a c-Met/Alk/

Ron/Ros multitargeted kinase inhibitor, has been clinically used for nonsmall-cell lung cancer (NSCLC).[13,24] Although both inhibitors got similar c-Met inhibitory activity, compound PF-04217903 adopted a different binding mode from Crizotinib in the ATP binding pocket, which may lead to their different selectivity.[22] Thus, to develop novel c-Met inhibitors with enhanced activity and selectivity, it is important to study the specific binding mode and structure−activity relationship (SAR) of the triazolopyrazines derivatives. 3D-QSAR models, including CoMFA[25] and CoMSIA,[26] provide straightforward information for SAR analysis of the compounds with the same or similar scaffolds. The structural and pharmacophoric information and their effects on activity derived from the 3D-QSAR models will assist further drug design.[27−32] In addition, molecular dynamics simulations enable better understanding about protein−ligand interactions. Moreover, molecular dynamics simulation studies on compounds with different selectivity will provide detailed information to explain and elucidate the mechanisms for improving selectivity.[33−36]

In the present study, molecular docking, 3D-QSAR modeling, molecular dynamics simulation, and binding free energy calculation were applied to investigate the detailed protein−ligand interactions of triazolopyrazine c-Met inhibitors. 3D-QSAR models, which were developed based on docking conformations, gave information on the effects of different interactive fields and structural requirements for highly active c-Met inhibitors. Molecular dynamics simulation, hydrogen bond occupancy analysis, and binding free energy calculations were also carried out on compounds with different selectivity bound to c-Met. Therefore, this study attempts to identify important structural and pharmacophoric features for enhancing c-Met inhibitory activity and specific mechanisms for improving c-Met selectivity. It will provide additional insights into potential structural modifications for developing more potent and selective c-Met inhibitors.

2. Computational Methods.

2.1. 3D-QSAR Study.

Data Set for 3D-QSAR Models. A total of 78 triazolopyrazine c-Met inhibitors, which covered reasonable chemical diversity and biological activity, were obtained from published data (Table S1 in the Supporting Information).[16−22] For developing 3D-QSAR models, the training and test set compounds should both span at least four orders of activity magnitude and be well-proportioned in each activity magnitude. With these basic rules, the compounds were manually divided into the training set and test set. The training set consisting of 28 compounds was used to develop the 3D-QSAR models and the test set contained the rest 50 compounds. Both sets took a reasonable distribution of the biological data. Their IC_{50} (nM) values were converted into pIC_{50} (9-$logIC_{50}$), which would be used as dependent variables for subsequent 3D-QSAR analysis.

Ligand Preparation and Alignment. 3D structures of the compounds were constructed within the sketch module, and atom types of each molecule were checked in Sybyl6.9. Using *Gasteiger-Hückel* charge assignment and Tripos standard force field parameters, the structures were energy minimized through 500 steps by applying the Powell method without constraints. Molecular alignment is the most sensitive factor which has a significant effect on the 3D-QSAR models. In this study, by simulating the binding conformations of the compounds, molecular alignment was obtained through molecular docking. Thus, all the molecules were well aligned in the binding site for developing 3D-QSAR models.

Molecular Docking. The crystal structure of c-Met kinase in complex with PF-04217903 (PDB ID: 3ZXZ) obtained from the protein data bank (PDB) was used for molecular docking with Glide 5.5 implemented in Schrödinger 2009.[37] The complex structure obtained was first prepared with the *Protein Preparation Wizard workflow*. All the water molecules were removed. The binding region was defined by a box centered on the centroid of the crystal ligand and in similar size with the ligand. The extra precision (XP) mode was used for the docking and scoring. All other parameters were kept default. The best pose was output on the basis of Glide score and the protein−ligand interactions.

3D-QSAR Model Construction. Both CoMFA and CoMSIA models were built using the QSAR module in Sybyl6.9. The standard Tripos force field was employed for CoMFA and CoMSIA analysis. To derive CoMFA descriptor fields, a hybridized sp^3 carbon atom with a charge of +1.0 and van der Waals radius of 1.53 Å was employed as a probe to compute the steric (S) and electrostatic (E) energies between the probe and the compounds. For CoMSIA analysis, by using a sp^3 carbon atom probe with a charge of +1.0, five similarity indices consisting of steric (S), electrostatic (E), hydrophobic (H), hydrogen bond donor (D), and hydrogen bond acceptor (A) fields were calculated for each lattice with a grid of 2 Å. The optimal number of components was designated so that cross-validated r^2_{cv} was maximal and the standard error of prediction was minimal. CoMSIA, using Gaussian-type distance dependence, provides smooth and interpretable contour maps. A default value of 0.3 was used as the attenuation factor.

Partial Least-Squares (PLS) Analysis. PLS analysis was used to linearly correlate the CoMFA and CoMSIA fields to the activity values. The descriptors of CoMFA and CoMSIA were used as independent variables, and pIC_{50} activity values were used as dependent variables. The cross-validation analysis was performed using the leave-one-out (LOO) method, in which one compound is removed from the data set, and its activity can be then predicted using the model derived from the rest compounds of the data set. The model resulting in the highest cross validated r^2_{cv}, optimum number of components (ONC), and the lowest standard error of prediction were taken for further analysis. To speed up the analysis and reduce noise, a minimum column filter value σ (2.00 kcal/mol) was used. A final analysis was performed to calculate conventional r^2_{ncv} to obtain the final QSAR models for CoMFA and CoMSIA using the ONC obtained from the cross-validation analysis. In addition, the statistical significance of the models was described by the standard error of estimate (SEE) and probability value (F value).

3D-QSAR Model Validation. The predictive capability of the 3D-QSAR models was evaluated with the external test set of 50 molecules. The test set molecules were also optimized and aligned in the same manner as described above, and their activities were predicted using the developed models. The predictive correlation (r^2_{pred}) based on the test set molecules is computed using eq 1

$$PRESS = \sum (Y_{actual} - Y_{predicted})^2$$

$$SD = \sum (Y_{actual} - Y_{mean})^2$$

$$r^2_{pred} = (SD - PRESS)/SD \tag{1}$$
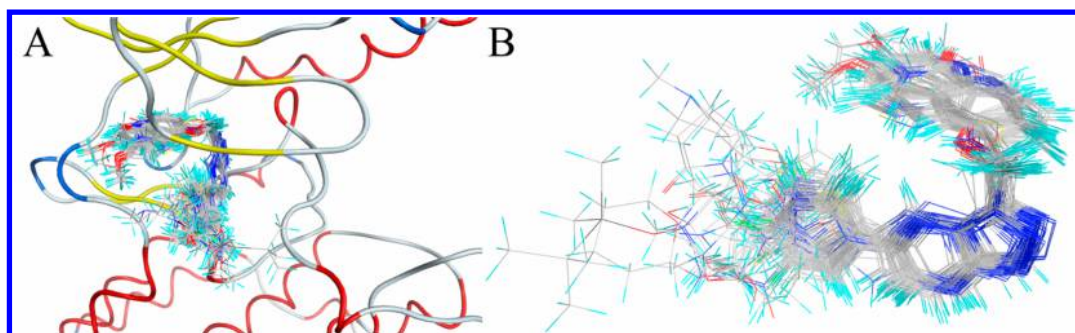
Figure 1. Molecular alignment based on the docking conformations. A) Alignment in the binding pocket; B) Alignment results for the 78 compounds from the training and test sets.

where $Y_{predicted}$, Y_{actual}, and Y_{mean} are the predicted, actual, and mean values of pIC_{50}. SD is the sum of the squared deviations between the biological activities of the test set and mean activities of the training set molecules, and PRESS is the sum of squared deviation between predicted and actual activity values for every molecule in the test set.

2.2. Molecular Dynamics Simulation. Molecular dynamics simulations were performed using the AMBER 9.0 software package with the ff99SB force field[38] to simulate c-Met in complex with its inhibitors and calculate their binding free energy. The cocomplex structures were obtained by molecular docking. The ligands were first fully minimized by the AM1 method and electrostatic potentials computed at the HF/6-31G* level in the Gaussian 09 program. The RESP fitting technique in AMBER was used to determine the partial charges. The force-field parameters for the ligand were generated with the general AMBER force field (GAFF) by the Antechamber program.[39] Hydrogen atoms were assigned using the LEaP module, which sets ionizable residues to their default protonation states at a neutral pH value. Each complex was immersed in a cubic box of TIP3P water model with a 10 Å minimum solute-wall distance.[40] A total of five Cl⁻ ions were added to neutralize each protein−ligand complex system. Energy was minimized in the solvated system employing 1000 steps of the steepest descent algorithm and 2000 steps of the conjugate gradient algorithm with a nonbonded cutoff of 10 Å. The protocol for molecular dynamics simulation consists of gradual heating, density equilibration, equilibration, and production procedures in an isothermal isobaric ensemble (NPT, $P = 1$ atm and $\mathbf{T} = 298$ K) MD. The system was gradually heated from 0 to 298 K in 50 ps, followed by density equilibration at 298 K for 500 ps, and then constant equilibration at 298 K for 500 ps. Then each protein−ligand complex system underwent a process of equilibration procedure until the system achieved a continuous stable status, i.e. production stage. The time step was set to 2 fs, while the snapshots were taken every 10 ps to record the conformation trajectory during production MD. The nonbonded interactions were treated with a 10 Å cutoff.[41] SHAKE algorithm[42] was applied to constrain all bonds involving hydrogen atoms to their equilibrium length. The conformations of different systems were collected every 50 ps after the system achieved their equilibrium status. The collected snapshots were used for structural and energetic analysis of each complex system.

Binding free energy calculations were also performed to investigate the differences of binding affinity between different ligands and the binding pocket. The methods like MM/PBSA[43] and MM/GBSA[44] are usually used for investigating the

energetic contribution of protein−ligand binding affinities. For different protein−ligand systems, the process of converged status was used for the binding free energy calculation. The solute and solvent dielectric constants were set as 1.0 and 80.0, respectively. The binding free energy of different ligands to the protein was calculated as follows:

$$\Delta G_{binding} = G_{complex} - [G_{protein} + G_{ligand}]$$

For different protein−ligand systems, the process for binding free energy calculations was also applied for hydrogen bond occupancy calculations. The hydrogen bond distance was set as 3.5 Å and the angle was 120.0°. Other parameters were kept default.

3. RESULTS AND DISCUSSION

3.1. 3D-QSAR Modeling. *Molecular Alignment.* The quality of 3D-QSAR models is sensitive to the molecular alignment because the inhibitory activities got strong correlation with different substitutions on a specific point in the same compound series. Molecular alignment based on the common structure has been widely applied; however, it is supposed to be more reasonable if the 3D-QSAR models could be constructed and evaluated on the active conformations of training and test set compounds. In the evaluation of docking programs, the best docking conformation predicted by Glide well reproduced the crystal conformation of compound PF-04217903 (RMSD = 0.4155), which was one of the triazolopyrazine c-Met inhibitors discussed in this study. With this crystal complex structure, all training and test set compounds were docked into the active site of c-Met, and the best pose for each compound is considered as the bioactive conformation, which was used for molecular alignment (Figure 1). Although the spatial positions of the scaffolds were not kept still in the alignment, they were in an acceptable range of displacement. Actually, this reflected the real situation that different bioactive conformations might be adopted by these derivatives due to various substituted groups. Besides, the alignment using docking conformations will also facilitate understanding the contour maps of the models in a structure-based manner.[31]

3D-QSAR Statistics. The 3D-QSAR CoMFA and CoMSIA models were constructed by Sybyl6.9. All the statistical parameters of the 3D-QSAR models were summarized in Table 2. The CoMFA model gave a cross-validated coefficient r^2_{cv} of 0.503 with an optimal component of 6, r^2_{ncv} of 0.983, SEE of 0.167, and F value of 201.100. The corresponding field contributions of parameters were 63.6% of the steric field and 36.4% of the electrostatic field descriptor, indicating a greater

influence of the steric field. The CoMSIA model developed based on five fields (S, E, H, D, and A), giving the cross-validated coefficient r^2_{cv} of 0.732 with an optimal components of 6, r^2_{ncv} of 0.988, SEE of 0.141, and F value of 283.710, was employed for detailed analysis. The corresponding field contributions were 6.8%, 21.9%, 24.4%, 27.8%, and 17.0% for steric, electrostatic, hydrophobic, hydrogen bond donor, and acceptor fields, respectively. It could be found that the hydrogen bond fields, including hydrogen bond donor and acceptor, made great contributions for the protein−ligand binding and c-Met inhibitory activity especially. These statistical parameters indicated that these two models were statistically significant (Table 1). Table S1 (Supporting Information)

Table 1. Statistical Parameters of the CoMFA and CoMSIA Models

statistical parameters	CoMFA	CoMSIA
r^2_{cv}[a]	0.503	0.732
ONC[b]	6	6
SEE[c]	0.167	0.141
r^2_{ncv}[d]	0.983	0.988
F-value[e]	201.100	283.710
r^2_{pred}[f]	0.733	0.947
fraction of field contributions		
steric	0.636	0.068
electrostatic	0.364	0.219
hydrophobic		0.244
hydrogen bond donor		0.278
hydrogen bond acceptor		0.170

[a]Leave-one-out (LOO) cross-validated correlation coefficient. [b]Optimum number of components. [c]Standard error of estimate. [d]Noncross-validated correlation efficient. [e]F-test value. [f]Predicted correlation coefficient for the test set.

includes the experimental and predicted pIC_{50} values and the residuals defined as the experimental minus the predicted pIC_{50} values. It could be found that they did not deviate significantly from each other (generally less than one logarithmic unit, Table S1). Figure 2 illustrated the strong linear correlations between experimental and predicted activities of the two models. The correlated coefficient values demonstrated their high internal predictability.

Validation of the 3D-QSAR Models. Besides, a test set of 50 c-Met inhibitors (marked by * in Table S1) was also used to further validate the external predictability. The CoMFA and CoMSIA models were applied to predict their activity. It could be found that the predicted pIC_{50} values agreed well with the experimental values in a tolerable error range. The predictive correlation coefficients r^2_{pred} were 0.733 and 0.947, respectively (Figure 2). Comparatively, the CoMSIA model showed better capability in predicting the activity of external compounds.

Contour Map. Since the steric and electrostatic contour maps obtained in CoMFA analysis were similar to that in CoMSIA, and the CoMSIA model showed better predictability, only 3D contour maps of the CoMSIA model were interpreted. Because the models were derived from the docking conformations, the contour maps could be easily aligned into the active site of c-Met kinase, which may provide deep insights into the protein−ligand interactions. Thus, the contour maps were discussed in combination with the 3D structure of c-Met with the ligand PF-04217903 and the protein surface to show different features of the site.

Steric contour maps gave the information about the spatial volume of substituted groups on different positions. There were three green and one yellow contour maps located in the active site, while green means bulky groups were favored and yellow means bulky groups were disfavored (Figure 3). The first medium green contour map appeared on the position of the adenine binding region (R_1), indicating that bulky groups in this region were suitable for improving activity (Figure 4). From the training and test set compounds, it could be found that compounds with R_1 of bicyclo-groups like quinoline generally got better activity than monocycle groups like benzyl, phenyl, or methoxybenzene. For example, compound **10** is almost 10 times more active than compound **7** (Figure S1 in the Supporting Information). The second green contour map covered the pyrazine ring, indicating bulky groups were suitable in this position. The other small green contour map was located in the head of the narrow channel to solvent accessible region, which was rimmed by Asp1164, Arg1208, Asn1209, Tyr1230, and Asp1231. Although it was limited crosswise, group R_2 could be inserted into this narrow but deep channel. Therefore, planar groups substituted in this position should be reasonable to increase the activity. The yellow contour map was located at the bottom of the triazole ring, deep in the binding pocket. This region was occupied by Asp1222, indicating that large substituted groups are not favorable.

For electrostatic contour maps, it was shown in combination with the electrostatic protein surface (Figure 3). It should be noted that from red to blue of the protein surface, the electrostatic was changed from most positive to negative, while
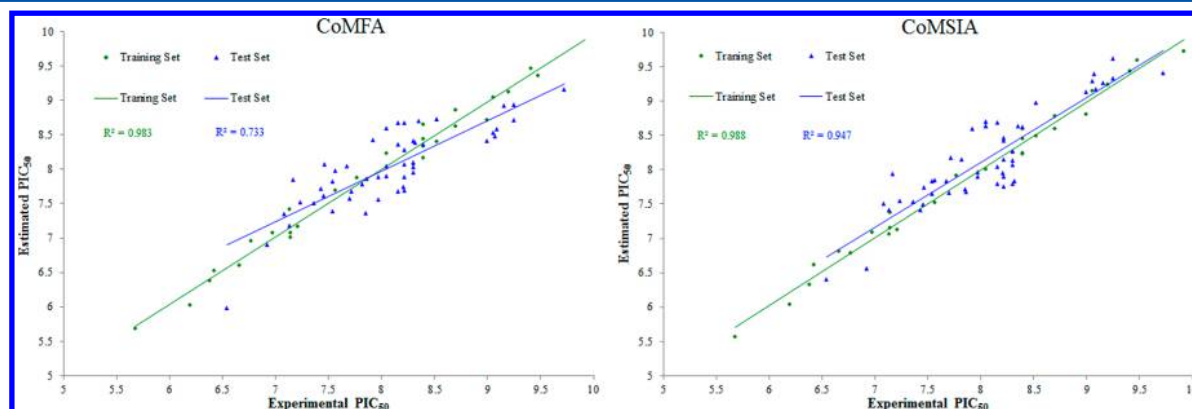
Figure 2. Correlation between the predicted and experimental activities of the training and test set compounds (CoMFA and CoMSIA models).
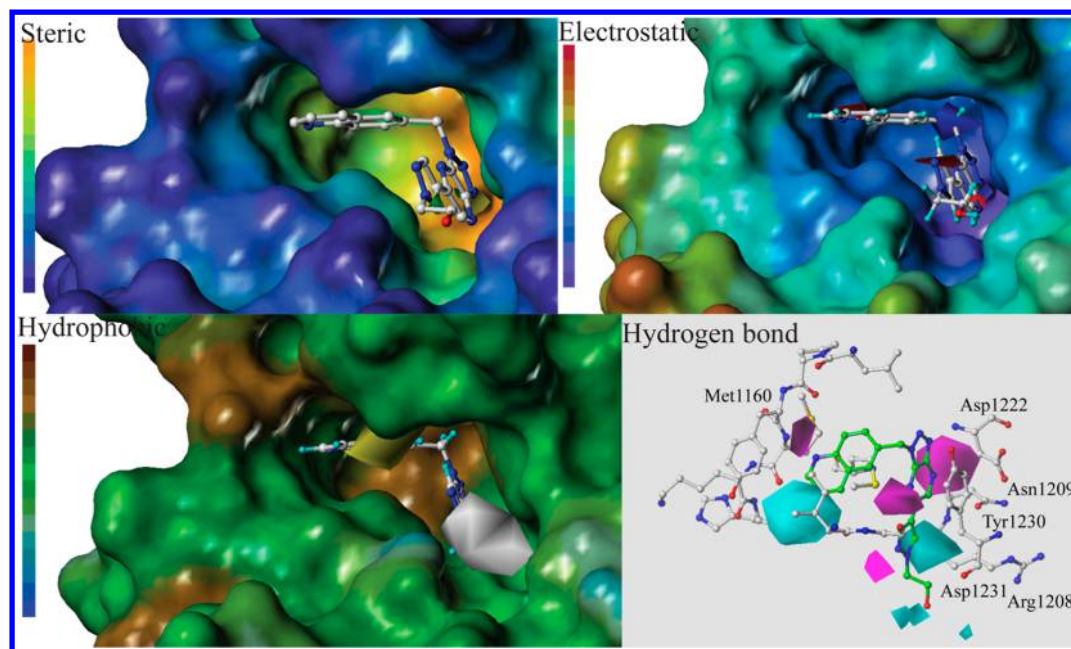
Figure 3. Contour maps were shown in combination of compound PF-04217903 in the background of protein surface (Steric: cavity depth surface; Electrostatic: electrostatic potential surface; Hydrophobic: lipophilic potential surface). Steric: Green contour maps indicate regions where bulky groups were favored for improving activity, whereas yellow ones meant bulky groups were not favored. The color from blue to red of cavity depth surface meant low to high depth inside the receptor. Electrostatic: Blue contour maps indicated regions where positive groups were beneficial for improving activity, whereas red ones meant negative groups were favored. The electrostatic potential surface was shown in color from purple (most negative) to red (most positive). Hydrophobic: Yellow contour maps (hydrophobic groups were favored); White (hydrophobic groups were disfavored). The lipophilic potential surface was shown in color from brown (highest hydrophobic) to blue (highest hydrophilic). The contour maps of hydrogen bond donor (HBD) and hydrogen bond acceptor (HBA) were shown in combination with compound PF-04217903. Cyan (HBD favored); purple (HBD disfavored); magenta (HBA favored); red (HBA disfavored).
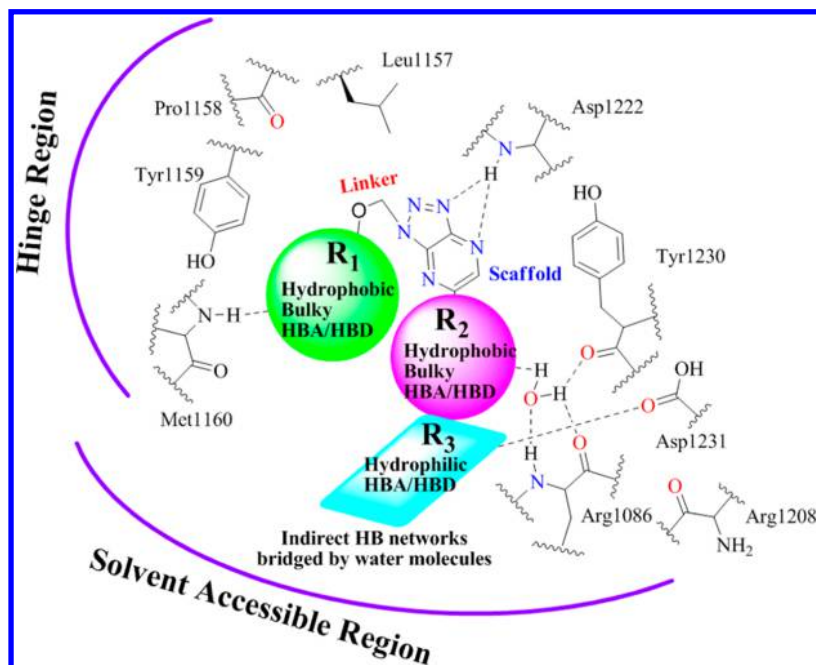
Figure 4. SAR summary in the presence of scaffold. HBA: Hydrogen Bond Acceptor; HBD: Hydrogen Bond Donor.

it was opposite for the CoMSIA contour map. The red contour map was found to cover the nitrogen atom of quinoline, indicating negative electrostatic groups here were beneficial for improving activity. Therefore, it was found in the training and test sets that there were other groups such as hydroxyl and oxygen atom of methoxyl substituted in this position. Another

red contour map covered neither nitrogen atom of the pyrazine ring, indicating positive electrostatic groups here were not suitable. The effect on activity could be evidently observed from compounds **39** and **40** (Figure S2 in the Supporting Information). The other red contour map covered the 2′-N of the pyrazole, indicating positive electrostatic groups were not

2548

dx.doi.org/10.1021/ci500268s | J. Chem. Inf. Model. 2014, 54, 2544−2554
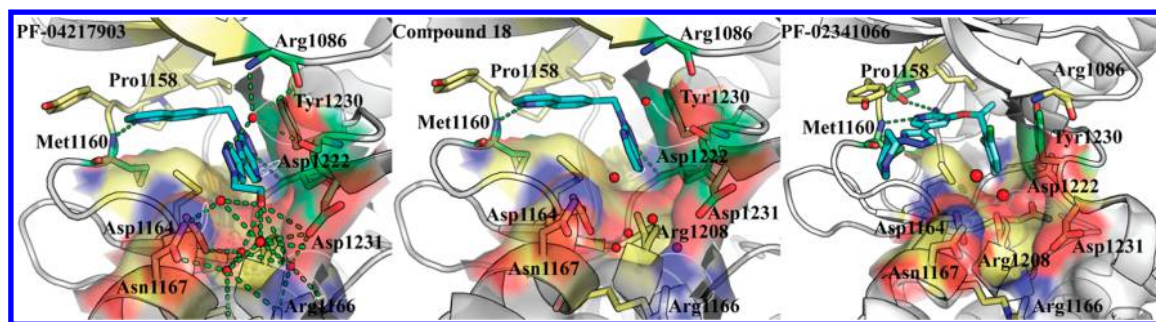
Figure 5. Binding modes of the three compounds (PF-04217903, compound **18**, and PF-02341066) in the c-Met active site shown in combination with the surface of the narrow channel.

suitable here. The amino acid residue Arg1086 with a positive charge was the nearest to this nitrogen atom. Therefore, this red contour map was consistent with the property requirements of the binding site. The only blue contour map covered the methylene linker. Because of the electrowithdrawing property of the three nitrogen atoms on the triazole ring, the methylene was comparatively positive. Activity of the compounds could be significantly improved like compounds **38**−**42** if another oxygen atom was added to the linker at the other side of the methylene because it improved the electropositivity of the methylene.

Hydrophobic contour map was shown in the background of the receptor lipophilic potential surface (Figure 3). There were two contour maps in the active site, one in the adenine binding region, and the other in the middle of the narrow channel described above. The yellow one indicated that hydrophobic groups were beneficial for improving activity, which was consistent with the color of the protein surface. Actually, R_1 groups in the adenine pocket were almost hydrophobic. Compounds with quinoline substituted here obviously got better activity than benzyl, phenyl, and methoxybenzene, indicating higher hydrophobic groups were more favorable. The white contour map located in the narrow channel was close to the solvent accessible region, indicating hydrophobic groups were not beneficial for improving activity. On the contrary, hydrophilic groups were favorable in the region close to the solvent accessible region. It could be found that the activity of compounds with hydrophilic groups substituted here were about 10 times better than those without such groups, like compounds PF-04217903 and **18** (Figure S3 in the Supporting Information). Therefore, hydrophilic groups are suggested to be beneficial for improving activity on this position.

Hydrogen bonds were also considered to be very important for the binding and activity of ligands. The hydrogen bond donor (HBD) and acceptor (HBA) contour maps were also provided by the CoMSIA model to facilitate structural optimization (Figure 3). First, cyan and magenta contour maps were in the proximity of R_1. The magenta contour map in the proximity of Met1160 illustrated that the hydrogen bond interaction between Met1160 and the ligand should be favored for improving c-Met inhibitory activity. For compound PF-04217903, the nitrogen atom of the quinoline ring formed a hydrogen bond with Met1160, agreeing well with the magenta contour map. The cyan contour map was also located between R_1 and the carbonyl oxygen atom of Met1160, indicating groups with a hydrogen bond donor were also beneficial for improving activity. This suggested that activity might be improved if the ligand provided one hydrogen bond to the carbonyl oxygen atom of Met1160. Another magenta contour

map of large volume appeared beneath the scaffold of triazolopyrazine. This is consistent with the hydrogen bonds between some ligands and the binding pocket. The two nitrogen atoms accepted hydrogen bonds from Asp1222, which is important for the binding and activity of c-Met inhibitors. Therefore, retaining these hydrogen bond acceptors is important in the process of structural optimization. Activity of compounds without such hydrogen bond acceptors, like compounds **74**−**78**, decreased significantly. The other two magenta contour maps appeared over the triazolopyrazine and the pyrazole ring. No direct hydrogen bonds were found in this region between the ligand and amino acid residues; but after the crystal water molecules were added, indirect hydrogen bonds could be bridged by them between the ligands and the nearby amino acid residues. Actually, indirect hydrogen bond interactions with residues in the channel should also be beneficial for increasing the selectivity as this region was less conservative in other kinases. Three other small hydrogen bond donor contour maps located in the terminal of the channel also reflected the fact that hydrophilic groups with a hydrogen bond donor should be beneficial for better activity. Hydrogen bond interactions between the hydroxyl of the ligand and the carbonyl oxygen atom of Asp1231 were observed. This was well consistent with the hydrogen bond donor contour map. The last cyan contour map was located beneath the pyrazole ring, over Arg1208. The carbonyl of Arg1208 was in the middle of the channel bottom. Ligands with a hydrogen bond donor group here are suggested to provide hydrogen bond interaction with the carbonyl.
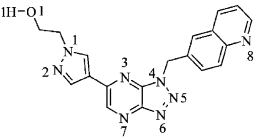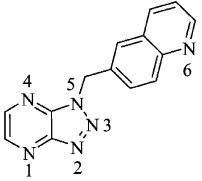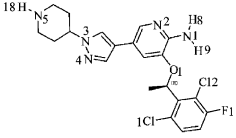
SAR Summary. The SAR information on different R groups was summarized in Figure 4. In the adenine binding pocket, bulky volume and hydrophobicity were preferable for R_1 groups, and hydrogen bond interactions were also very important between R_1 and the hinge residues. Apart from the existing hydrogen bond forming between the nitrogen atom of quinoline and NH of Met1160, one more hydrogen bond between the carbonyl oxygen atom of Met1160 and R_1 may be favorable for further activity improvement. Linker is the key part for ligands to keep the "U"-shaped conformation, and −O−CH$_2$− was suggested to be the most suitable group. For the scaffold, the hydrogen bond with Asp1222 was considered as one of the most important protein−ligand interactions. Therefore, the hydrogen bond acceptors on the scaffold should be kept in the process of structural optimization. As R_2 is located in the head of the narrow but deep channel, planar bulky groups inserted into the channel lengthwise were favored. The R_2 group with one hydrogen bond donor and acceptor is preferred to interact with Arg1208 and Arg1086, respectively. Group R_3 extended to solvent accessible region and got
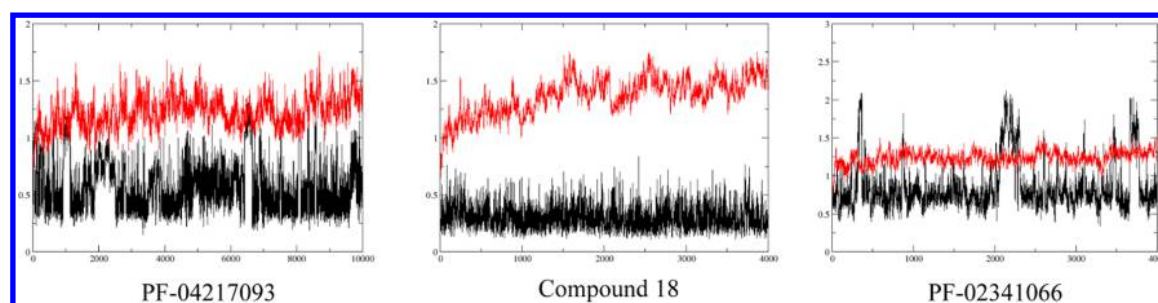
Figure 6. Changes of the backbone of protein (red line) and ligands (black line) in the process of the molecular dynamics simulations, vertical axis represented RMSD values, and horizontal axis represented time of the simulation (unit: picosecond).

Table 2. Hydrogen Bond Occupancy of Three Compounds (PF-04217903, Compound 18, and PF-02341066) and Solvent Molecules in the Selected Phase of Molecular Dynamics Simulations

Compd.	H-bond		Occupied (%)
PF-04217903	N8@MOL	Met1160:NH	98.80
	N6@MOL	Asp1222:NH	65.45
	OH@MOL	Asp1231:OD1	61.25
	N7@MOL	Asp1222:NH	52.20
	OH@MOL	Asp1231:OD2	2.85
	OH@MOL	Asp1164:OD2	1.15
	OH@MOL	Asp1164:OD1	0.05
	N2@MOL	solvent	155.95
	O1@MOL	solvent	148.45
Compound 18	N6@MOL	Met1160:NH	98.75
	N2@MOL	Asp1222:NH	93.90
	N1@ MOL	Asp1222:NH	19.60
	OH@ MOL	Asp1231:OD2	2.85
	OH@ MOL	Asp1164:OD2	1.15
	OH@ MOL	Asp1164:OD1	0.05
	N4@MOL	solvent	18.10
PF-02341066	N1H8@MOL	Pro1158:O	99.50
	N2@MOL	Met1160:NH	99.45
	F1@ MOL	Asp1222:NH	32.55
	Cl2@ MOL	Asp1222:NH	0.25
	N5@MOL	solvent	117.55
	solvent	N5H18@MOL	80.65
	N4@MOL	solvent	63.05

interactions with the solvent molecules. Observed from the results, this channel could be considered as a hydrogen bond rich region, as dense hydrogen bond networks were found among the ligands, residues, and solvent molecules (Figure 5). Thus, groups R$_2$ and R$_3$ may contribute to the binding and activity of this series of c-Met inhibitors. As these effects could not be observed from the results of the 3D-QSAR models, molecular dynamics simulations were performed to illustrate the differences between compounds with and without substituted groups in this hydrogen bond rich region.

3.2. Molecular Dynamics Simulations. Compared to PF-04217903, compound **18** lacks substituents in the hydrogen bond rich region (Figure 5), and there is about 15-fold activity difference. To investigate the effect on activity made by substituents in the hydrogen bond rich region (R$_2$ and R$_3$), compounds **18** and PF-04217903 were selected to conduct the molecular dynamics simulation. Binding free energy calculation

and hydrogen bond occupancy analysis of these two compounds will provide the detailed information about the differences between them.

Compound PF-04217903 has similar c-Met inhibitory activity with PF-02341066; however, their selectivity is significantly different. Although both of them were bound in the ATP binding pocket, they extended to solvent accessible regions in different directions (Figure 5). Therefore, in order to understand the effect on selectivity made by their different extending directions, molecular dynamics simulation, hydrogen bond occupancy analysi,s and binding free energy calculation were also performed on the protein−ligand system of c-Met with PF-02341066.

*Comparison of PF-04217903 and Compound **18**.* To explore the dynamic stability of the system, the root-mean-square-deviation (RMSD) values using the starting structure as a reference were calculated (Figure 6). In the process of a 10 ns

Table 3. Binding Free Energy Calculated Using MM/PBSA and MM/GBSA Methods

contribution	PF-04217903		compound 18		PF-02341066	
	mean/(kcal/mol)	std	mean/(kcal/mol)	std	mean/(kcal/mol)	std
ΔE_{ele}	−30.59	6.97	−19.11	2.29	−14.49	2.30
ΔE_{vdw}	−54.41	2.27	−38.09	1.73	−52.01	2.56
ΔE_{intra}	0.00	0.00	0.00	0.00	0.00	0.00
ΔE_{gas}	−84.99	6.79	−57.19	2.55	−66.51	3.39
ΔG_{pbsur}	−6.37	0.35	−4.82	0.25	−6.31	0.26
ΔG_{pbcal}	55.86	4.27	33.68	2.19	32.32	3.21
ΔG_{pbsol}	49.49	4.36	28.86	2.21	26.01	3.19
ΔG_{pbele}	25.28	4.10	14.57	1.79	17.83	2.41
ΔG_{pbtot}	−35.50	3.57	−28.34	1.62	−40.50	2.91
ΔG_{gbsur}	−6.37	0.35	−4.82	0.25	−6.31	0.26
ΔG_{gb}	48.14	5.30	28.34	1.70	27.00	2.09
ΔG_{gbsol}	41.77	5.45	23.52	1.74	20.69	2.07
ΔG_{gbele}	17.55	2.43	9.23	1.24	12.51	1.57
ΔG_{gbtot}	−43.22	2.29	−33.67	1.58	−45.82	2.77

molecular dynamics simulation on c-Met in complex with PF-04217903, both of the receptor and ligand's RMSD plots showed some fluctuation, but the overall actual values were very small. It could be found that the backbone of the receptor fluctuated in the range of 1−1.5 Å, and the ligand changed in the range of 0.25−1 Å, indicating the system stayed in an equilibrated and converged stage and kept stable. It could be also found that the protein−ligand system has reached a stable stage from other aspects (Figure S4 in the Supporting Information), including density, energy, pressure, and temperature. B factor (Figure S5 in the Supporting Information) of the receptor was also predicted by the simulation. Little changes were found on the conserved amino acid residues in the process of the simulation, like the hinge region (103−105 on the horizontal axis), Asp1222 (167 on the horizontal axis) and Tyr1230 (175 on the horizontal axis), indicating that the ligand binding site was also kept in a stable conformation. Considering the fluctuation of the RMSD values shown in Figure 6, the process from 7 to 9 ns was taken for the analysis of hydrogen bond occupancy (Table 2) and binding free energy calculation. The occupancy rate of the hydrogen bond with Met1160 reached 98%. Besides, the occupancy rate of the hydrogen bonds between Asp1222 and the scaffold (N6 and N7) reached 65.45% and 52.20%, respectively. Besides, another stable hydrogen bond was observed between Asp1231 and the hydroxyl group of R_3, the occupancy rate of which reached 61.25%. Analysis of hydrogen bonds between the ligand and solvent molecules also showed a high occupancy rate. Therefore, consistent with the conclusion with the CoMSIA contour maps of hydrogen bonds, this region could be considered as a hydrogen bond rich region.

For compound 18, the protein−ligand system reached the converged stage early at about 1.5 ns (Figure 6). The macroscopic variables, including density, energy, pressure, and temperature, also showed the protein−ligand system reached the equilibrated and stable stage (Figure S6 in the Supporting Information). The backbone of receptor fluctuated around 1.5 Å, and the ligand changed in the range of 0.25−0.5 Å (Figure 6). Meanwhile, the B factor predicted by this simulation also showed the conserved amino acid residues kept in a stable conformation (Figure S7 in the Supporting Information). Hydrogen bond analysis of compound 18 with the receptor (Table 2) showed that it kept stable interactions with Met1160 and Asp1222. Without substituted groups in the hydrogen

bond rich region, no stable hydrogen bonds were formed between the ligand and residues of the narrow channel or the solvent molecules (Table 2).

Binding free energy was calculated for these two compounds using MM/PBSA and MM/GBSA methods (Table 3), respectively. Binding free energy was considered to reflect the binding affinity of the ligands. Compound PF-04217903 got more favorable ΔPBTOT and ΔGBTOT values than compound 18, indicating PF-04217903 got higher binding affinity with binding pocket. This was consistent with the activity differences between these two compounds. On the basis of their structural differences, R_2 and R_3 groups in the hydrogen bond rich region contributed mainly to the deviations of the binding affinity.

Considering all above, compounds PF-04217903 and 18 got almost the same interactions with the receptor except the hydrogen bond rich region (Figure 5), indicating substituents in the hydrogen bond rich region are essential to improve the binding and activity. Stable hydrogen bonds will be generated between these substituted groups and the hydrogen bond rich region and solvent molecules. Therefore, structural optimization in the hydrogen bond rich region may be a reasonable solution to improve c-Met inhibitory activity.

Comparison of PF-04217903 and PF-02341066. The RMSD plots (Figure 6) of the protein−ligand system for PF-02341066 showed that the backbone of the receptor fluctuated in the range of 1−1.5 Å from the beginning, and the ligand normally changed in the range of 0.5−1 Å, indicating the system stayed in an equilibrated and converged stage and kept stable. It could be found that there were some fluctuations of the ligand conformation during the process. We extracted and compared the ligand conformations with the highest and normal RMSD values. It was found that the fluctuations were mainly caused by the regular tiny rotation of the piperidine on PF-02341066 (Figure S8 in the Supporting Information). Therefore, the RMSD values fluctuated regularly to some degree but were not bigger than 2.0 Å. Other aspects of the system also illustrated that it kept a stable status in the process of molecular dynamics simulation (Figure S9 in the Supporting Information). The B factor predicted also illustrated that the conserved amino acid residues were kept in a stable conformation (Figure S10 in the Supporting Information). Therefore, the complex system of PF-02341066 and c-Met kinase domain was considered to be converged within the

simulation time. Hydrogen bond analysis and binding free energy calculation were also performed. From Table 3, two hydrogen bonds were generated between the ligand and hinge region amino acid residues (Pro1158 and Met1160). The occupancy rates were 99.50% and 99.45% (Table 2), indicating they were stable for ligand binding. Hydrogen bond interactions between the ligand and solvent molecules with high occupancy rates were also favored for ligand binding, but no other stable hydrogen bonds between the ligand and binding pocket were found. Other hydrogen bond interactions formed between the substituted groups on the phenyl and Asp1222 were far from being stable for the protein−ligand binding.

PF-04217903 has been reported as a highly active and selective type I c-Met inhibitor, while PF-02341066 was highly active but less selective, which was a c-Met/Alk/Ros/Ron multitargeted inhibitor. Since both of them bound to the ATP binding pocket in a "U"-shaped conformation, it made great sense to analyze their binding modes in detail to find out what made the differences on their selectivity. Their binding free energy calculated using MM/PBSA and MM/GBSA were consistent with their activity values (Table 3). The hydrophobicity of the binding pocket was also suggested by the calculations, where the absolute value of the ΔE_{vdw} term (−54.41 kcal/mol, −52.01 kcal/mol) were greater than that of thte ΔE_{ele} term (−30.59 kcal/mol, −14.49 kcal/mol). It could be also concluded from these values that these two compounds got similar hydrophobic interactions with the binding pocket, but the electrostatic interactions made the major difference. The substituted phenyl of PF-02341066 and the scaffold of PF-04217903 formed π−π stacking interactions with the electron rich Tyr1230. Due to the different electron deficiency of these two fragments, the strength of π−π stacking interactions was also different. The scaffold of triazolopyrazine showed more electron deficiency than the substituted benzene, leading to a stronger π−π stacking interaction between Tyr1230 and PF-04217903 than PF-02341066.[22]

Besides the differences made by π−π stacking interactions, hydrogen bond interactions with the binding pocket also played an important role. From the results of hydrogen bond analysis, both of them formed stable hydrogen bonds with the hinge region residues, which were considered to be very important for kinase inhibitors' binding. Observed from other known inhibitors, it was common that one hydrogen bond between the ligand and hinge region also satisfied the requirements although PF-04217903 got no hydrogen bonds with Pro1158. PF-04217903 also formed stable hydrogen bonds with Asp1222. The nitrogen atoms on the scaffold made great contributions to these two hydrogen bonds; but for PF-02341066, the chloride and fluorine atoms could not form stable hydrogen bonds with Asp1222, the occupancies of which were both under 50% (Table 2). Furthermore, because of their different binding modes, they approached the solvent accessible region from different directions (Figure 5). R_2 and R_3 of PF-02341066 extended into the solvent accessible region from the ligand entrance region nearby the hinge region. Hydrogen bond networks were formed between the ligand and solvent molecules (Table 2). Although it was reported that hydrogen bonds between the ligand and residues of the ligand entrance region were favored for improving selectivity,[45] no such hydrogen bonds were found with PF-02341066 (Table 2). For PF-04217903, the tail groups substituted in the narrow channel also got stable hydrogen bonds with the solvent

molecules. Indirect hydrogen bond networks with the residues bridged by water molecules were also found (Figure 5); but different with PF-02341066, there was another stable hydrogen bond with Asp1231, which was one of the amino acid residues constituted the narrow channel. Therefore, substituted groups located in this hydrogen bond rich region made the differences on selectivity between these two compounds.

Comparison of the Binding Pockets. Considering the substituents in the hydrogen rich region made the main differences on the selectivity, it makes great sense to investigate the corresponding region of other kinases targeted by PF-02341066 like Alk/Ron/Ros to compare with c-Met. The crystal structures of PF-02341066 in complex with Alk (PDB ID: 2XP2)[13] and Ros (PDB ID: 3ZBF)[46] and Ron in complex with AMP-PNP (PDB ID: 3PLS)[47] are available. From the protein surface (Figure 7), although there is a pocket for the substituted phenyl of PF-02341066, there was no such narrow channel as that in the binding pocket of c-Met, indicating that this narrow channel was special and different from other kinases. The substituted phenyl of PF-02341066 well fitted into the small pocket of other kinases, leading to its high activity against them and less selectivity for c-Met. Meanwhile, the small pocket of other kinases was not bulky enough for the binding of PF-04217903, while the narrow channel of c-Met accommodated R_2 and R_3 groups well, resulting in its high selectivity and activity for c-Met. Consequently, this distinctive narrow channel was important for improving the selectivity of the inhibitors. Besides, this channel was also found in the binding pocket of the dually phosphorylated activated state of c-Met. Although the conformation of the activation loop changed due to phosphorylation, the residues of Arg1208, Asn1209, Met1211, Asp1222, Asp1164, and Arg1166 still hold the channel. Since the spatial positions of residues like Tyr1230 and Asp1231 constituted the wall of the channel changed, another hydrophilic pocket neighboring the channel appeared for groups to occupy. This new orientation has been also studied in detail in our published paper.[31] The compounds with groups substituted in the channel and following this new orientation also got good inhibitory activity against the mutant types of c-Met.

In summary, despite the differences made by the π−π stacking interactions with Tyr1230, the stable hydrogen bond interactions should be a strong supplement to the explanation for the high selectivity of PF-04217903. The indirect hydrogen bonds bridged by the solvent molecules with the narrow channel also greatly contributed. All these hydrogen bonds with the narrow channel residues were located in the special hydrogen bond rich region identified from the 3D-QSAR analysis, indicating the importance of this region for improving the selectivity.

4. CONCLUSIONS

3D-QSAR modeling and molecular dynamics simulations were performed on c-Met inhibitors of the triazolopyrazine series in this study. The CoMFA and CoMSIA models were constructed with the docking conformations of training set compounds. The statistics demonstrated their reliability and significant predictive ability, especially the CoMSIA model. Furthermore, from contour maps of the CoMSIA model, structural and pharmacophoric feature requirements were obtained for different groups substituted on the scaffold. It is worth noting that an important hydrogen bond rich region was identified by the contour maps. Molecular dynamics simulations were

performed to assess the contributions to ligand binding, activity, and selectivity made by substituted groups in the hydrogen bond rich region. Comparison between the results of PF-04217903 and compound **18** confirmed that it was important to have suitable substituted groups in this region for developing highly active type I c-Met inhibitors. Meanwhile, by comparing the results of PF-04217903 and PF-02341066, hydrogen bond networks formed in this region, also greatly contributed to their selectivity. The results of this study will facilitate the research and development of highly active and selective type I c-Met inhibitors.

■ ASSOCIATED CONTENT

ⓢ Supporting Information

Table S1 and Figures S1−S10. This material is available free of charge via the Internet at http://pubs.acs.org.

■ AUTHOR INFORMATION

Corresponding Authors

*Phone: 86-25-86185163. Fax: 86-25-86185182. E-mail: ydchen@cpu.edu.cn (Y.C.).
*Phone: 86-25-86185086. Fax: 86-25-83302827. E-mail: lutao@cpu.edu.cn (T.L.).

Notes

The authors declare no competing financial interest.

■ ACKNOWLEDGMENTS

■ REFERENCES

(1) Birchmeier, C.; Birchmeier, W.; Gherardi, E.; et al. Met, metastasis, motility and more. *Nat. Rev. Mol. Cell Biol.* **2003**, *4*, 915−925.

(2) Di Renzo, M. F.; Narsimhan, R. P.; Olivero, M.; et al. Expression of the Met/HGF receptor in normal and neoplastic human tissues. *Oncogene* **1991**, *6*, 1997−2003.

(3) Ma, P. C.; Tretiakova, M. S.; MacKinnon, A. C.; et al. Expression and mutational analysis of MET in human solid cancers. *Genes, Chromosomes Cancer* **2008**, *47*, 1025−1037.

(4) Boccaccio, C.; Comoglio, P. M. Invasive growth: a MET-driven genetic programme for cancer and stem cells. *Nat. Rev. Cancer* **2006**, *6*, 637−645.

(5) Migliore, C.; Giordano, S. Molecular cancer therapy: can our expectation be MET? *Eur. J. Cancer* **2008**, *44*, 641−651.

(6) Maulik, G.; Shrikhande, A.; Kijima, T.; et al. Role of the hepatocyte growth factor receptor, c-Met, in oncogenesis and potential for therapeutic inhibition. *Cytokine Growth Factor Rev.* **2002**, *13*, 41−59.

(7) Wilson, T. R.; Fridlyand, J.; Yan, Y.; et al. Widespread potential for growth-factor-driven resistance to anticancer kinase inhibitors. *Nature* **2012**, *487*, 505−509.

(8) Turke, A. B.; Zejnullahu, K.; Wu, Y. L.; et al. Preexistence and clonal selection of MET amplification in EGFR mutant NSCLC. *Cancer Cell* **2010**, *17*, 77−88.

(9) Straussman, R.; Morikawa, T.; Shee, K.; et al. Tumour microenvironment elicits innate resistance to RAF inhibitors through HGF secretion. *Nature* **2012**, *487*, 500−504.

(10) Engelman, J. A.; Zejnullahu, K.; Mitsudomi, T.; et al. MET amplification leads to gefitinib resistance in lung cancer by activating ERBB3 signaling. *Science* **2007**, *316*, 1039−1043.

(11) Eder, J. P.; Vande Woude, G. F.; Boerner, S. A.; et al. Novel therapeutic inhibitors of the c-Met signaling pathway in cancer. *Clin. Cancer Res.* **2009**, *15*, 2207−2214.

(12) Gherardi, E.; Birchmeier, W.; Birchmeier, C.; et al. Targeting MET in cancer: rationale and progress. *Nat. Rev. Cancer* **2012**, *12*, 89−103.

(13) Cui, J. J.; Tran-Dube, M.; Shen, H.; et al. Structure based drug design of crizotinib (PF-02341066), a potent and selective dual inhibitor of mesenchymal-epithelial transition factor (c-MET) kinase and anaplastic lymphoma kinase (ALK). *J. Med. Chem.* **2011**, *54*, 6342−6363.

(14) Underiner, T. L.; Herbertz, T.; Miknyoczki, S. J. Discovery of small molecule c-Met inhibitors: Evolution and profiles of clinical candidates. *Anticancer Agents Med. Chem.* **2010**, *10*, 7−27.

(15) Porter, J. Small molecule c-Met kinase inhibitors: a review of recent patents. *Expert Opin. Ther. Pat.* **2010**, *20*, 159−177.

(16) Albrecht, B. K.; Harmange, J. C.; Bauer, D.; et al. Discovery and optimization of triazolopyridazines as potent and selective inhibitors of the c-Met kinase. *J. Med. Chem.* **2008**, *51*, 2879−2882.

(17) Boezio, A. A.; Berry, L.; Albrecht, B. K.; et al. Discovery and optimization of potent and selective triazolopyridazine series of c-Met inhibitors. *Bioorg. Med. Chem. Lett.* **2009**, *19*, 6307−6312.

(18) Chen, F.; Wang, Y.; Ai, J.; et al. O-linked triazolotriazines: potent and selective c-Met inhibitors. *ChemMedChem.* **2012**, *7*, 1276−1285.

(19) Ryu, J. W.; Han, S. Y.; Yun, J. I.; et al. Design and synthesis of triazolopyridazines substituted with methylisoquinolinone as selective c-Met kinase inhibitors. *Bioorg. Med. Chem. Lett.* **2011**, *21*, 7185−7188.

(20) Ye, L.; Ou, X.; Tian, Y.; et al. Indazoles as potential c-Met inhibitors: design, synthesis and molecular docking studies. *Eur. J. Med. Chem.* **2013**, *65*, 112−118.

(21) Ye, L.; Tian, Y.; Li, Z.; et al. Design, synthesis and molecular docking studies of some novel spiro[indoline-3,4′-piperidine]-2-ones as potential c-Met inhibitors. *Eur. J. Med. Chem.* **2012**, *50*, 370−375.

(22) Cui, J. J.; McTigue, M.; Nambu, M.; et al. Discovery of a novel class of exquisitely selective mesenchymal-epithelial transition factor (c-MET) protein kinase inhibitors and identification of the clinical candidate 2-(4-(1-(quinolin-6-ylmethyl)-1H-[1,2,3]triazolo[4,5-b]-pyrazin-6-yl)-1H-pyrazol-1-yl)ethanol (PF-04217903) for the treatment of cancer. *J. Med. Chem.* **2012**, *55*, 8091−8109.

(23) Yuan, H.; Lu, T.; Ran, T.; et al. Novel strategy for three-dimensional fragment-based lead discovery. *J. Chem. Inf. Model.* **2011**, *51*, 959−974.

(24) Cui, J. J. Targeting Receptor Tyrosine Kinase MET in Cancer: Small Molecule Inhibitors and Clinical Progress. *J. Med. Chem.* **2014**, *57*, 4427−4453.

(25) Cramer, R. D.; Patterson, D. E.; Bunce, J. D. Comparative molecular field analysis (CoMFA). 1. Effect of shape on binding of steroids to carrier proteins. *J. Am. Chem. Soc.* **1988**, *110*, 5959−5967.

(26) Klebe, G.; Abraham, U.; Mietzner, T. Molecular similarity indices in a comparative analysis (CoMSIA) of drug molecules to correlate and predict their biological activity. *J. Med. Chem.* **1994**, *37*, 4130−4146.

(27) Leng, Y.; Lu, T.; Yuan, H. L.; et al. QSAR studies on imidazopyrazine derivatives as Aurora A kinase inhibitors. *SAR QSAR Environ. Res.* **2012**, *23*, 705−730.

(28) Lu, S.; Liu, H. C.; Chen, Y. D.; et al. Combined pharmacophore modeling, docking, and 3D-QSAR studies of PLK1 inhibitors. *Int. J. Mol. Sci.* **2011**, *12*, 8713−8739.

(29) Ran, T.; Lu, T.; Yuan, H.; et al. A selectivity study on mTOR/PI3Kalpha inhibitors by homology modeling and 3D-QSAR. *J. Mol. Model.* **2012**, *18*, 171−186.

(30) Yuan, H.; Liu, H.; Tai, W.; et al. Molecular modelling on small molecular CDK2 inhibitors: an integrated approach using a combination of molecular docking, 3D-QSAR and pharmacophore modelling. *SAR QSAR Environ. Res.* **2013**, *24*, 795−817.

(31) Yuan, H.; Tai, W.; Hu, S.; et al. Fragment-based strategy for structural optimization in combination with 3D-QSAR. *J. Comput.-Aided. Mol. Des.* **2013**, *27*, 897−915.

(32) Zhang, Y.; Liu, H.; Jiao, Y.; et al. De novo design of N-(pyridin-4-ylmethyl)aniline derivatives as KDR inhibitors: 3D-QSAR, molecular fragment replacement, protein-ligand interaction fingerprint, and ADMET prediction. *Mol. Diversity* **2012**, *16*, 787−802.

(33) Chang, H. W.; Chung, F. S.; Yang, C. N. Molecular modeling of p38alpha mitogen-activated protein kinase inhibitors through 3D-QSAR and molecular dynamics simulations. *J. Chem. Inf. Model.* **2013**, *53*, 1775−1786.

(34) Huang, Y. Y.; Li, Z.; Cai, Y. H.; et al. The molecular basis for the selectivity of tadalafil toward phosphodiesterase 5 and 6: a modeling study. *J. Chem. Inf. Model.* **2013**, *53*, 3044−3053.

(35) Sabbah, D. A.; Vennerstrom, J. L.; Zhong, H. A. Binding selectivity studies of phosphoinositide 3-kinases using free energy calculations. *J. Chem. Inf. Model.* **2012**, *52*, 3213−3224.

(36) Roy, K. K.; Saxena, A. K. Structural basis for the beta-adrenergic receptor subtype selectivity of the representative agonists and antagonists. *J. Chem. Inf. Model.* **2011**, *51*, 1405−1422.

(37) Kontoyianni, M.; McClellan, L. M.; Sokol, G. S. Evaluation of docking performance: comparative data on docking algorithms. *J. Med. Chem.* **2004**, *47*, 558−565.

(38) Duan, Y.; Wu, C.; Chowdhury, S.; et al. A point-charge force field for molecular mechanics simulations of proteins based on condensed-phase quantum mechanical calculations. *J. Comput. Chem.* **2003**, *24*, 1999−2012.

(39) Wang, J.; Wang, W.; Kollman, P. A.; et al. Automatic atom type and bond type perception in molecular mechanical calculations. *J. Mol. Graphics Modell.* **2006**, *25*, 247−260.

(40) Jorgensen, W. L.; Chandrasekhar, J.; Madura, J. D.; Impey, R. W.; Klein, M. L. Comparison of simple potential functions for simulating liquid water. *J. Chem. Phys.* **1983**, *79*, 926−935.

(41) Darden, T.; York, D.; Pedersen, L. Particle mesh Ewald, Particle mesh Ewald: An N·log(N) method for Ewald sums in large systems. *J. Chem. Phys.* **1993**, *98*, 10089−10092.

(42) Ryckaert, J.-P.; Ciccotti, G.; Berendsen, H. Numerical Integration of the Cartesian Equations of Motion of a System with Constraints: Molecular Dynamics of n-Alkanes. *J. Comput. Phys.* **1977**, *23*, 327−341.

(43) Kollman, P. A.; Massova, I.; Reyes, C.; et al. Calculating structures and free energies of complex molecules: combining molecular mechanics and continuum models. *Acc. Chem. Res.* **2000**, *33*, 889−897.

(44) Onufriev, A.; Bashford, D.; Case, D. A. Exploring protein native states and large-scale conformational changes with a modified generalized born model. *Proteins* **2004**, *55*, 383−394.

(45) Liao, J. J. Molecular recognition of protein kinase binding pockets for design of potent and selective kinase inhibitors. *J. Med. Chem.* **2007**, *50*, 409−424.

(46) Awad, M. M.; Katayama, R.; McTigue, M.; et al. Acquired resistance to crizotinib from a mutation in CD74-ROS1. *N. Engl. J. Med.* **2013**, *368*, 2395−2401.

(47) Wang, J.; Steinbacher, S.; Augustin, M.; et al. The crystal structure of a constitutively active mutant RON kinase suggests an intramolecular autophosphorylation hypothesis. *Biochemistry* **2010**, *49*, 7972−7974.

2554

dx.doi.org/10.1021/ci500268s | *J. Chem. Inf. Model.* 2014, 54, 2544−2554